Resource Coloring Allocation for Managing Grating Lobes in Distributed Satellite Configuration

1st Giulio Orlando
Thales Alenia Space
Toulouse, France
giulio.orlando@thalesaleniaspace.com

2nd Francesco Lisi
Thales Alenia Space
Heriot-Watt University
Toulouse, France
f.lisi@hw.ac.uk

3rd Margaux Pellet
Heriot-Watt University
Edinburgh, UK
mp2026@hw.ac.uk

4th Thomas Delemotte
University of the Bundeswehr Munich
Neubiberg, Germany
thomas.delamotte@unibw.de

5th George Goussetis
Heriot-Watt University
Edinburgh, UK
G.Goussetis@hw.ac.uk

6th Hervé Legay
Thales Alenia Space
Toulouse, France
herve.legay@thalesaleniaspace.com

***Abstract*—This paper investigates the advantages of multi-spot beam satellite networks, which can leverage power and bandwidth gains through efficient resource management. Efficient resource allocation is essential to reduce losses and improve utilization in satellite systems that operate under resource limitations. Recent developments in satellite technology have considerably increased the feasibility of delivering high-demand services to users. Traditionally, these services are managed by allocating resources through ground stations, which control and distribute communication resources (such as bandwidth and power) between satellites and users. This study focuses on downlink Frequency Division Multiple Access (FDMA) in satellite-terrestrial networks, analyzing an aperture antenna in space communicating with user terminals (UTs) under two Direct Radiating Array (DRA) payload configurations: continuous and fractionated. The fractionated approach allows a collaborating distributed platform to form a complete radiating surface, however introducing challenges such as grating lobes. The research examines the performance of bandwidth allocation among UTs in the same spot beam on overall system capacity. To mitigate interference from grating lobes, an optimization strategy is proposed. The results highlight significant capacity improvements, emphasizing the critical role of effective bandwidth management in enhancing network performance.**

***Index Terms*—Direct radiating array, fractionated antenna, grating lobes, colouring resource allocation.**

I. Introduction

As the space industry undergoes rapid evolution, the concept of constructing a distributed antenna array from multiple satellites acting as a cohesive aperture is gaining significant attention. This innovative approach is particularly relevant in the era of mega-constellations and has a critical role in enhancing satellite communication capabilities. The increasing demand for higher throughput and efficient frequency reuse in point-to-point satellite communications is driving the exploration of multibeam systems, alongside the development of supporting technologies. To address the challenges posed by spatially uneven and time-varying traffic across satellite coverage areas, various technologies have emerged to facilitate flexible payload resource allocation. Key advancements include digital on-board processors, beam hopping, adaptive coding and modulation, flexible power allocation per beam, and active antennas. Moreover, recent developments in Direct-to-Cell (D2C) communication are becoming a pivotal area of focus. D2C technologies are set to play an increasingly significant role in the future of satellite communication, as they allow for direct communication between satellites and end users without relying on ground stations. This shift will place additional pressure on radio resource management, requiring more efficient solutions to fully exploit the scarce spectrum and guarantee high-quality service for end users. As highlighted in the 3GPP standards, particularly in 3GPP TR 38.811 (NR for Future Wireless Networks) [1], efficient radio resource allocation will be critical for maintaining quality of service (QoS) in systems with high user demand and limited spectrum resources. The synergy between satellite-based multibeam systems and D2C technologies calls for advanced resource allocation strategies to ensure the optimal use of available spectrum, especially as these systems scale up. This need for effective Resource Management (RM) strategies is highlighted in recent works. For instance, in [2], the heuristic Reuse Resource Management (H-RRM) algorithm has demonstrated performance comparable to the more computationally intensive Mixed Integer Quadratic Programming (MIQP) approach, while maintaining linear complexity relative to the number of users. This makes it a promising solution for optimizing resource allocation in satellite networks. However, as satellite systems transition towards distributed architectures with multiple antennas and beams, interference from grating lobes—manifesting throughout the entire field of view—becomes a significant concern. In such systems, this interference can degrade performance and complicate the task of efficient resource allocation. To address this, a suitable algorithm has been developed to either avoid or account for the presence of grating lobes in the performance calculations. Through comprehensive computer simulations, the effectiveness of these RRM techniques has been evaluated

within multi-beam satellite systems under progressively denser uniform traffic scenarios.

This paper is structured as follows: Section II presents the system model, detailing the downlink and traffic frameworks; Section III introduces the theory of beam orthogonality; Section IV describes the proposed RRM algorithms; Section V discusses extensive simulation results across various traffic conditions; and Section VI concludes with a summary and key insights drawn from the study.

Notations: notation R is used as a subscript (pedix) to indicate the receiving condition, while T denotes the transmitting one. $\mathbf{A}(i,:)$ and $\mathbf{A}(:,j)$ denote all the elements in row i and all the elements in column j, respectively. $\widehat{\mathbf{A}}$ represents the normalized version of the matrix $\mathbf{A}$. $[\mathbf{A}]^a$ indicates a column selection of the matrix $\mathbf{A}$. $[\mathbf{A}]_a$ indicates a row selection of the matrix $\mathbf{A}$. $\mathbf{x}^{\mathrm{c}}$ denotes a vector of signals operating at a specific color frequency c. $\mathbf{A}^{\mathrm{c_R},\mathrm{c_T}}$, in the context of a transmission between two devices, denotes a generic matrix referred to the specific condition of transmitting at color frequency $\mathrm{c_T}$ towards a specific receiving color frequency $\mathrm{c_R}$.

II. System Model

The space segment is composed of a platform equipped with a phased array that provide communication over a designated ground service area. The continuous aperture consists of N_{T} radiating elements arranged into $N_{\mathrm{x}}N_{\mathrm{y}}$ subarrays, each containing $M_{\mathrm{x}}M_{\mathrm{y}}$ elements. The spacing between elements inside a single subarray is set at $\lambda/2$, where λ is the wavelength of the carrier signal. To simulate aperture fractionation, the distance d (in units of λ) between subarrays is varied, offering flexibility in the system's architecture, as illustrated in Fig. 1. The satellite's Field of View (FoV) is the region where the User Terminal maintains Line of Sight (LOS) with the satellite at an elevation angle above 25 degrees, as per the assumptions. With this condition in the scenario, the satellite in LEO at 600Km of orbit altitude has a FoV $= 56$.

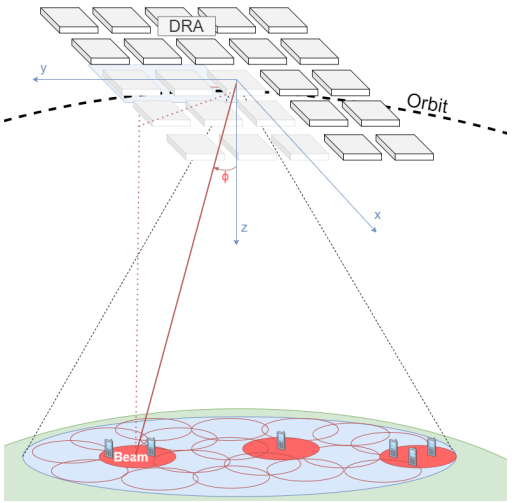

Fig. 1: System Architecture.

A random, uniform distribution of users is assumed within the satellite's FoV to model different user terminal densities. The distribution radius, denoted as R, governs the density of user terminals, allowing simulation across a range of low to high-density scenarios (Fig. 2). Each UT location in the FoV is defined by spherical coordinates (θ, ϕ), representing the angle of departure of the signal from the array's center to the user's position [4]. The phased array of N_T radiating elements on the satellite operates in the S band in accordance with the sub-6GHz frequency bands for the sixth generation of mobile communication technology.

The DRA design is developed across three levels: array, subarray, and radiating element. This setup allows each subarray to function as an orbiting platform, increasing the overall radiating surface. The elementary source is defined by a theoretical cosine diagram, given by the equation:

$$\mathrm{EP}(\theta) = 10^{D/20} \cdot \cos\left(\frac{\pi\theta}{2 \cdot 2\frac{\pi}{3}}\right)^n \tag{1}$$

with D as the directivity of the elementary patch and n a natural number.

The coordinate system depicted in Fig. 2 satisfies the following relationships:

$$\begin{aligned} u_i &= \sin(\theta_i)\cos(\phi_i) \quad & \theta_i &= \sqrt{u_i^2 + v_i^2} \\ v_i &= \sin(\theta_i)\sin(\phi_i) \quad & \phi_i &= \tan^{-1}(v_i/u_i) \end{aligned} \tag{2}$$

Note that there is no one-to-one relationship between (θ, ϕ) and (u, v), since, for example, all pairs $(0, \phi)$ lead to $u = 0$ and $v = 0$. Nevertheless, each pair (u, v) corresponds to a unique direction of the upper half-space $z \geq 0$.

III. Beams Orthogonality

In antenna design, particularly in multibeam configurations, the concept of "nulls" in the radiation pattern is critical. A null refers to a point where the antenna's radiation pattern exhibits minimal energy. These nulls occur at specific directions relative to the antenna, where the emitted power is nearly zero or very low. In a rectangular grid arrangement, these null positions can be used strategically to organize the placement of the beams. The regular, grid-like structure of the nulls, is determined by the arrangement of the radiating elements in the DRA. The pattern of nulls effectively determines where beams can be placed with minimal interference, displaying spots where signals from different beams are least likely to overlap and cause disruption. However, when the DRA aperture is fractionated—that is, the antenna aperture is divided into smaller, discrete elements—this arrangement can lead to issues like grating lobes. Grating lobes are unwanted, periodic replicas of the main beam that can interfere with the signal. They arise when the spacing between radiating elements is too large relative to the wavelength of the transmitted signal. This improper element spacing causes multiple occurrences of the main beam to appear at regular intervals. In the proposed scenario, grating lobes are considered when their power exceeds -10 dB relative to the peak of the main beam, as they can reach significant levels and potentially cause

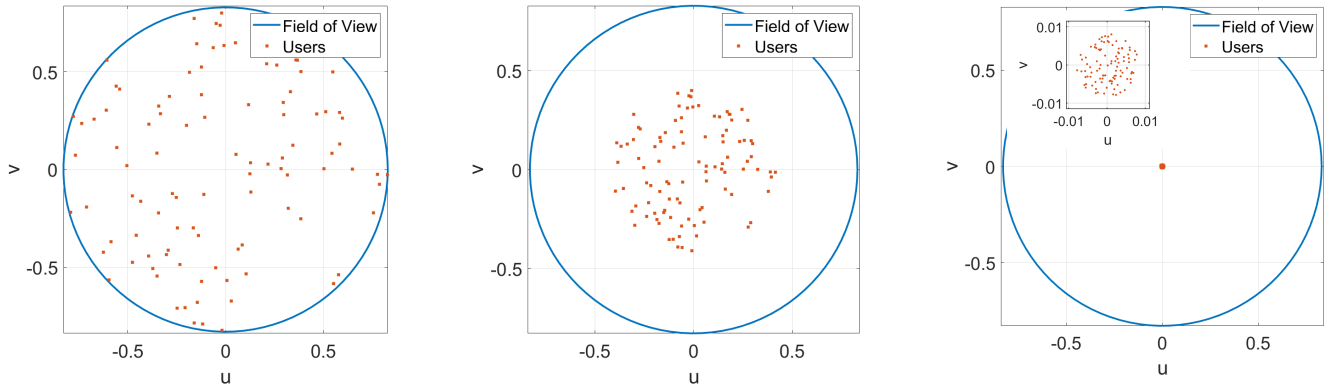

(a) $R_{user} = 100\%$. (b) $R_{user} = 50\%$. (c) $R_{user} = 1\%$ + Zoom.

Fig. 2: Different users distribution density over the FoV.

interference to user terminals operating in the direction of the grating lobes.

Therefore, it is crucial to manage the spacing of the radiating elements and the grid pattern to avoid these problematic lobes. The relationship between the grid periodicity and the placement of grating lobes is important (Eq.3):

$$\begin{aligned} u_m &= u_0 + m\tfrac{\lambda}{d_x} \quad m = 0, \pm 1, ... \\ v_n &= v_0 + n\tfrac{\lambda}{d_y} \quad n = 0, \pm 1, ... \end{aligned} \tag{3}$$

d_x and d_y represent the element distance in the x and y direction respectively; the grating lobes will appear at specific directions aligned with the grid, offset from the main beam's direction by multiples (m, n) of the wavelength divided by the element spacing (λ/d). As the antenna's main beam (u_0, v_0) is electronically scanned, the locations of the grating lobes also move. They maintain a fixed offset relative to the main beam's direction, ensuring that the grating lobes track with the main beam. This means that if the main beam is electronically steered to a new direction, the grating lobes will follow the beam's movement with an offset proportional to an integer multiple of λ/d.

Fig. 3 illustrates two scenarios of grid configurations for a fractionated DRA where a beam is allocated at the center null

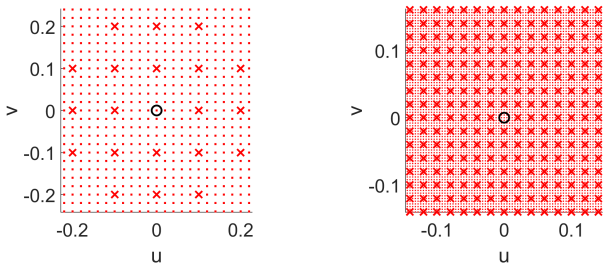

(a) $d = 10\lambda$ (b) $d = 50\lambda$

Fig. 3: Grid of fractionated DRA with grating lobes(×).

of the radiation pattern. The figure also shows the emergence of grating lobes, marked with an '×' symbol.

Fig. 3 leads to two main conclusions. On the positive side, increasing the distance between the subarray platforms allows for a denser grid of nulls within the same surface area. However, this also results in a significant increase in the number of generated grating lobes. If additional beams are strategically placed at the nulls surrounding the main beam the grating lobes will align with the same null distribution pattern, as illustrated in Fig. 4. Grating lobes are typically stronger when closer to the main central beam, due to the inherent characteristics of the radiation pattern associated with elementary radiating elements, especially those exhibiting a cosine shape. (Eq. 1). In an FDMA method for resource allocation, the available frequency band is divided into sub-bands, each being assigned a specific color-scheme. These color-schemes are defined as orthogonal, meaning they can operate simultaneously without interfering with each other. The number of sub-bands available for establishing a link depends on factors such as the user terminal's hardware capacity [10] and the density of user terminals in the spot beam. In this article, an example is provided using 9 colors, which is sufficient to cover the distribution of users and produce reasonable results. Although simulations with different numbers of colors have been conducted, their outcomes exceed the scope of this article. With 9 colors, it is possible to generate 9 multi-orthogonal grids shifted to allow the system to select the most suitable color to serve each user terminal (see Fig. 5) [8].

IV. System Capacity

To model the system of a generic DRA transmitting proper precoded signals $\mathbf{y}$ through N_T radiating elements towards N_U users on the ground, the following equation should be solved:

$$\mathbf{z} = \sqrt{P_T} \cdot \mathbf{H}\widehat{\mathbf{W}}\mathbf{x} + \mathbf{n}, \tag{4}$$

with the precoded signals defined as:

$$\mathbf{y} = \sqrt{P_T} \cdot \widehat{\mathbf{W}}\mathbf{x}. \tag{5}$$

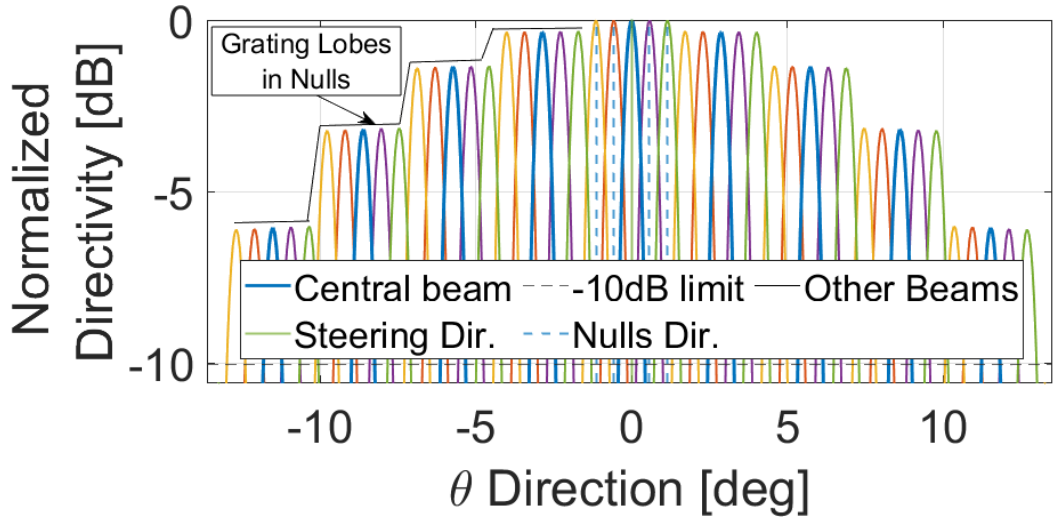

Fig. 4: Example multi beams allocated to nulls position for DRA Fractionated, $d = 10\lambda$. [3]

The input signals, the transmitted signals and the received signals can be collected in the column vectors $\mathbf{x} = [x_1, ..., x_j, ..., x_{N_U}]^T$, $\mathbf{y} = [y_1, ..., y_i, ..., y_{N_T}]^T$ and $\mathbf{z} = [z_1, ..., z_n, ..., z_{N_U}]^T$, where x_j , y_n and z_i are the complex input signal for user *j*, the complex signals transmitted by radiating element *n* and the complex signal received by receiver *i*, respectively.

The parameters involved are:

- complex matrix **H** (dimensions $N_U \times N_T$): The transfer function between the input ports of the N_T antenna radiating elements and the N_U user receiver. The generic entry element $h_{i,n}$ describes the complex transfer function between the input of the transmit radiating element *n* and the input of the user *i* receiver.
- complex transfer matrix **W** (dimensions $N_T \times N_U$): Express the relationship between signals at the input ports and the signals at the output ports of the precoding/beamforming OBP. The generic matrix element $w_{n,j}$ describe the complex transfer function between the input port *j* and output port *n*. The normalization of the precoding/beamforming matrix plays an important role in properly accounting for practical payload limitations such as the per antenna element power limitation affecting the DRA architecture.
- **n** is a vector whose elements represent the random noise process (thermal plus possible external inter-system interference) experienced by the N_U user.
- P_T : overall RF payload power.

The following assumptions stands for all the modeling of the system:

1) The distribution of users N_U on the FoV on Earth is already known.
2) Symbols in **x** are statistically independent.
3) The antennas have no mutual-coupling.
4) All users experience the same noise power.
5) Frequency colors are orthogonals.

Considering a population of N_U users that has to be serviced by the satellite forward-link and assuming that a precoding/beamforming technique is applied to the full population of users, the $N_U \times N_U$ normalized power transfer matrix **S** can be expressed as:

$$\mathbf{S}_{u_R} = P_T \left| \left[\mathbf{H}\right]_{u_R} \left[\widehat{\mathbf{W}}\right]^{u_R} \right|^2 \tag{6}$$

And it can be normalized over noise power $N = k_B T_s R_s$ as follow:

$$\widehat{\mathbf{S}} = \frac{\mathbf{S}}{k_B T_s R_s} \qquad \widehat{\mathbf{H}} = \frac{\mathbf{H}}{\sqrt{k_B T_s R_s}} \tag{7}$$

with T_s is the user antenna temperature, K_B is the Boltzmann constant, R_s is the symbol rate.

The element $s(i, j)$ of the matrix **S** denotes the power transmitted to the *j*-th user and received by the *i*-th user, normalized by the thermal noise power. The diagonal entries of **S** represent the useful transmission, quantified by the signal-to-noise ratio (SNR). In contrast, the off-diagonal entries indicate unwanted interference that needs to be minimized. By examining the *i*-th row of **S**, excluding its diagonal entry, the aggregate interference-to-noise ratio (INR) experienced by the *i*-th user can be determined. Similarly, the off-diagonal elements in the *j*-th column describe the power leaked by the antenna patterns of the *i*-th user in unintended directions, also normalized by the noise power. The matrix **S** is generally non-symmetric. Given this power transfer matrix, the resource management problem is formulated as a color assignment problem. This can be expressed as a $0-1$ integer programming problem using the binary entries of a coloring matrix. Let N_C denote the predefined number of colors. The binary coloring

matrix $\mathbf{C}$, with dimensions $N_{\mathrm{U}} \times N_{\mathrm{C}}$, is introduced to represent the allocation of resources:

$$\mathbf{C} = \begin{vmatrix} 0 & 1 & \cdots & 0 \\ 1 & 0 & \cdots & 0 \\ \vdots & \vdots & \ddots & \vdots \\ 0 & 0 & \cdots & 1 \end{vmatrix} \tag{8}$$

It is possible to think of the matrix $\mathbf{H}$ with dimensions $N_{\mathrm{U}} \times N_{\mathrm{T}}$ as a 4D matrix with dimensions $N_{\mathrm{U}} \times N_{\mathrm{T}} \times N_{c_R} \times N_{c_T}$, where $\mathrm{c_R}$ is the frequency color in reception form a user and $\mathrm{c_T}$ is the frequency color in transmission from the DRA. Thus the $\mathbf{H}$ matrix (or $\mathbf{W}$ matrix) related to a specific couple of colors can be identified as $\mathbf{H}^{\mathrm{c_R},\mathrm{c_T}}$. Following the assumption that each color is independent, $\mathbf{H}^{\mathrm{c_R},\mathrm{c_T}}$ can be expressed as $\mathbf{H}^{\mathrm{c_R},\mathrm{c_T}} \cdot \delta_{\mathrm{c_R},\mathrm{c_T}}$, with the Kronecker delta $\delta_{\mathrm{c_R},\mathrm{c_T}}$ defined as:

$$\delta_{\mathrm{c_R},\mathrm{c_T}} = \begin{cases} 1, & \text{if} \quad \mathrm{c_R} = \mathrm{c_T} \\ 0, & \text{if} \quad \mathrm{c_R} \neq \mathrm{c_T} \end{cases}$$

The signal received at the color frequency $\mathrm{c_R}$ becames:

$$\mathbf{z}^{\mathrm{c_R}} = \sqrt{P_{\mathrm{T}}} \sum_{\mathrm{c_T}} \sum_{\mathrm{u_T}} \mathbf{H}^{\mathrm{c_R},\mathrm{c_T}} \mathbf{C}_{\mathrm{u_T},\mathrm{c_T}} \left[\widehat{\mathbf{W}}^{\mathrm{c_T}}\right]^{\mathrm{u_T}} \mathbf{x}_{\mathrm{u_T}} + \mathbf{n}^{\mathrm{c_R}} \tag{9}$$

- $\mathbf{C}$ is an $N_{\mathrm{U}} \times N_{\mathrm{C}}$ matrix, where each row contains only zeros except for the entry corresponding to the served user (row) at the assigned color (column), which is equal to 1.
- $\mathbf{C}_{\mathrm{u_T},\mathrm{c_T}}$ is a scalar that equals 1 if user $\mathrm{u_T}$ is served by color $\mathrm{c_T}$, and 0 otherwise.
- $\mathbf{H}^{\mathrm{c_R},\mathrm{c_T}}$ is an $N_{\mathrm{U}} \times N_{\mathrm{T}}$ matrix associated with the color pair $(\mathrm{c_R}, \mathrm{c_T})$.
- $\widehat{\mathbf{W}}$ is an $N_{\mathrm{T}} \times N_{\mathrm{U}}$ normalized matrix representing the beamforming weights.
- $\left[\widehat{\mathbf{W}}^{\mathrm{c_T}}\right]^{\mathrm{u}}$ is a column vector containing the beamforming weights for a generic user.
- $\left[\widehat{\mathbf{W}}^{\mathrm{c_T}}\right]^{\mathrm{u_T}}$ is a column vector containing the beamforming weights specific to user $\mathrm{u_T}$.

The Signal-to-Noise Ratio, Interference-to-Noise Ratio, and the Signal-to-Noise-plus-Interference Ratio (SNIR) for the *i*-th user, related to the $\mathbf{S}$ matrix normalized to noise power N, can be expressed as:

$$\mathrm{SNR}_{\mathrm{u_R}} = \sum_{\mathrm{c_R}} \mathbf{C}_{\mathrm{u_R},\mathrm{c_R}} \widehat{\mathbf{S}}^{\mathrm{c_R},\mathrm{c_R}}_{\mathrm{u_R},\mathrm{u_R}} \tag{10}$$

$$\mathrm{INR}_{\mathrm{u_R}} = \sum_{\mathrm{c_T},\mathrm{c_R}} \sum_{\mathrm{u_T} \neq \mathrm{u_R}} \mathbf{C}_{\mathrm{u_R},\mathrm{c_R}} \mathbf{C}_{\mathrm{u_T},\mathrm{c_T}} \widehat{\mathbf{S}}^{\mathrm{c_R},\mathrm{c_T}}_{\mathrm{u_R},\mathrm{u_T}} \tag{11}$$

$$N_{\mathrm{u_R}} = 1 \tag{12}$$

To calculate the capacity of the system, the final signal-to-noise-plus-interference ratio (SNIR) referred to the receiving user $\mathrm{u_R}$ can be defined as:

$$\mathrm{SNIR}_{\mathrm{u_R}} = \frac{\mathrm{SNR}_{\mathrm{u_R}}}{\mathrm{INR}_{\mathrm{u_R}} + 1} \tag{13}$$

The Shannon capacity available for user $\mathrm{u_R}$ is given by:

$$C_{\mathrm{u_R}} = B_{\mathrm{u_R}} \cdot \log_2 \left(1 + \mathrm{SNIR}_{\mathrm{u_R}}\right) \tag{14}$$

The resource allocation algorithm focuses on defining the binary coloring matrix $\mathbf{C}$ and managing how much bandwidth $B_{\mathrm{u_R}}$ is available for a generic receiving user $\mathrm{u_R}$, as discussed in the next chapter. [2]

V. Resource Beam-User Allocation

The resource allocation algorithm is outlined in Algorithm 1. The algorithm takes two primary inputs: the number of colors (N_{C}) and the number of users (N_{U}), where the users' positions are given in the u-v coordinate system. While the user distribution is uncontrollable and follows a non-uniform statistical pattern, it may also exhibit clustering due to areas of high user density, or "hot spots."

An additional input, P, represents a set of grid points, spaced to maintain the orthogonality of the beams and their reciprocal allocation in a null position. Each color is associated with its own set of grid points. To improve computational efficiency, the algorithm only selects the grid points that are closest to the users for each color ($s^{(c)}$).

The primary objective of the algorithm is to construct the coloring matrix, which determines which grid point will serve as the beam center for each color to serve a user. Each grid point can have one of three states: Null, Beam, or Grating Lobe. Initially, all grid points are in the Null state. As iterations progress, the selected grid point for a user is marked as a Beam, and the surrounding grid points are designated as Grating Lobes based on their proximity to the beam.

The selection of a grid point to serve as the beam center is primarily based on distance (Fig. 5a). The closest grid point for each color is the first candidate to be selected as a Beam (Fig. 5b). However, in cases where multiple Grating Lobes are present at a given grid point, the algorithm may choose the second closest grid point to minimize interference. If only one Grating Lobe is present at a grid point, the algorithm allocates a beam to that point but splits the available bandwidth in half, allowing two beams of the same color to operate simultaneously without interference, despite their shared Grating Lobes.

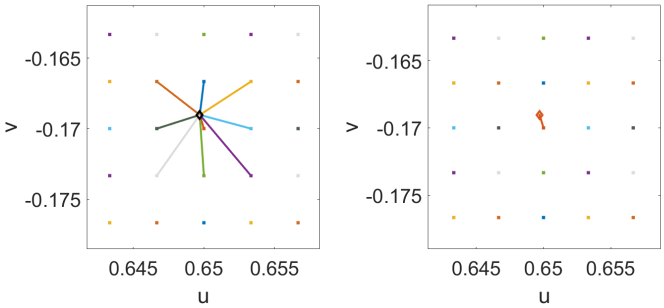

(a) User closest grids distances. (b) Closest grid point chosen.

Fig. 5: Zoom of grids colors points.

Algorithm 1: Colouring resource allocation

Inputs:
N_{C}, Number of colors
N_{U}, Number of users
U position users in u-v coordinates
P grid points of possible beam allocation for each colors in u-v coordinates
Outputs:
C, Colouring matrix
Initialize:
for user $= 1 : N_U$ **do**
  $s^{(c)} \leftarrow |P - U|_2$;
  $k^{(n)} \leftarrow \min(s^{(c)})$;
  $u^{(n)} \leftarrow \text{user}^{(n)}$;
  1) **if** $p(u^{(n)}, k^{(n)})$ is a Null **then**
    $c(u^{(n)}, k^{(n)}) \leftarrow 1$;
    $p(u^{(n)}, k^{(n)}) \leftarrow$ Beam;
    $p(u^{(n)}, k^{(n)}, gl) \leftarrow$ Grating lobes;
  else
    if $p(u^{(n)}, k^{(n)})$ is a Beam **then**
      $c(u^{(n)}, k^{(n)}) \leftarrow 1$;
    else
      if $p(u^{(n)}, k^{(n)})$ is a Grating lobe **then**
        count(gl);
        if count$(gl) \leq 1$ **then**
          $c(u^{(n)}, k^{(n)}) \leftarrow 1$;
          $p(\text{user}^{(n)}, \text{color}^{(n)}) \leftarrow$ Beam;
          $p(u^{(n)}, k^{(n)}, gl) \leftarrow$ Grating lobes;
          $\text{BW}_{\text{beam}} \leftarrow \text{BW}_{\text{beam}}/2$
        else
          $P_{\text{reduced}} \leftarrow \text{remove}(\text{color}^{(n)}, P)$;
          $s^{(c)} \leftarrow |P_{\text{reduced}} - U|_2$;
          $k^{(n)} \leftarrow \min(s^{(c)})$;
          Repeat Point 1;
        end
      end
    end
  end
end

VI. Results

To evaluate the performance of the proposed algorithm in a multibeam satellite system, we have enhanced the satellite multibeam simulator using the parameters detailed in Table I.

The plot in Fig. 6, illustrates how capacity (in Mbps) improves with an increase in the fractionation applied to the antenna structure. This improvement is found to be more significant in areas with higher user density, as highlighted in the plot by the x-axis parameter *R*. This parameter quantifies the spatial distribution of users within the FoV, provides a way to measure how concentrated or spread out users are across the FoV. The concentration is represented as a percentage, where 100% corresponds to a uniform distribution of users across the entire FoV, and lower percentages correspond to a more concentrated distribution of users. The system capacity was evaluated across four scenarios: one using a continuous DRA and four employing fractionated DRAs with separation distances of $d = 5\lambda$, $d = 10\lambda$, $d = 20\lambda$, and $d = 50\lambda$. A total of 100 users were randomly and uniformly distributed across the system area.

TABLE I: Parameters simulation

Parameter	Value
Frequency	2.19 GHz
N. radiating elements	900
N. radiating elements per subarray	6x6
N. subarrays	5x5
N. colors	9
Bandwidth	30 MHz
Bandwidth per color	Bandwidth/N.colors
G/T	20 dB
Altitude	600 Km
N. users	100

The findings are summarized as follows:

- **Low user density** ($R = 100\%$): The Continuous and Fractionated DRA configuration achieve the similar capacity, benefiting from an optimized arrangement of orthogonal beams. All configurations use the same number of beams in the optimal scenario of 1 user per beam.
- **Moderate user density** ($R = 50\%$): As user density continues to decrease, all Fractionated DRA configurations surpass the Continuous DRA in capacity. Meanwhile, the Continuous DRA allocates fewer beams as density decreases, highlighting a shift in resource utilization.
- **Higher user density** ($R = 20\%$): The Continuous DRA experiences a sharp drop in capacity as the user distribution becomes denser, requiring each beam to serve multiple users simultaneously.
- **Very high user density** ($R < 10\%$): At very low values of R, user density becomes sufficiently high within each beam, resulting in a substantial capacity drop. However, the configuration with $d = 50\lambda$ maintains high capacity and a significant number of active beams, even at $R = 1\%$.

The output of the algorithm revealed that the Coloring matrix **C** was not fully optimized in terms of utilizing all available colors. Specifically, after the first iteration, the users assigned to each color were distributed unevenly, as shown in Fig. 7a.

Building on this principle, an additional constraint was introduced, limiting the maximum number of users each color can serve. This allowed the algorithm to redistribute users across all colors, optimizing capacity utilization (see Fig. 7b).

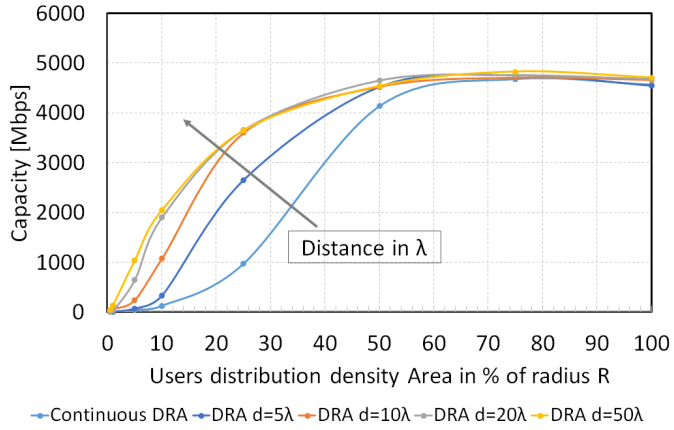

Fig. 6: System capacity vs. user distribution density (%).

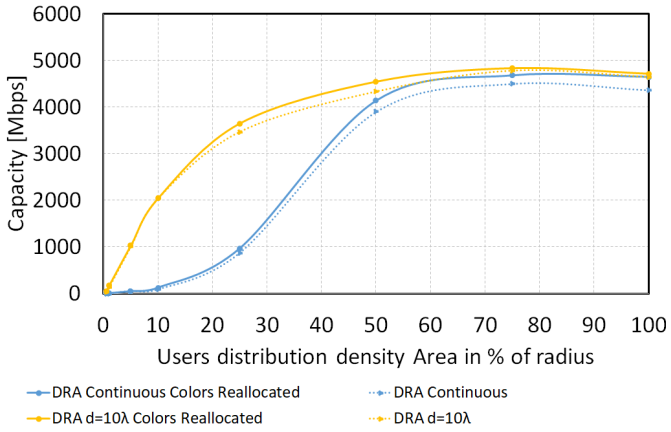

Fig. 8: Impact of color redistribution on capacity.

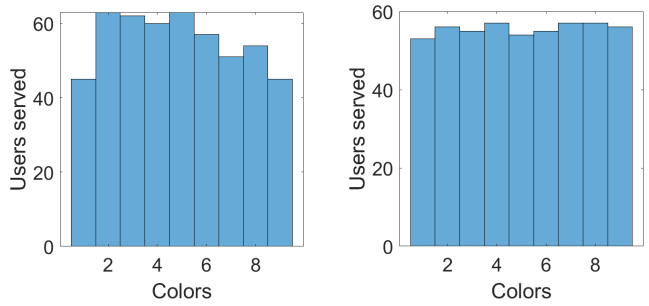

(a) Colors allocation unbalanced. (b) Colors allocation balanced.

Fig. 7: Comparison of colors allocation.

The per-color limit was defined by the rule N_U/N_C. A final plot in Fig. 8 can be created to compare the impact on capacity with and without the redistribution of users across the available colors. A slight improvement in capacity is observed when the users are redistributed.

VII. Conclusion

This paper presented a strategy for managing the emergence of grating lobes when analyzing a distributed antenna architecture. It demonstrates how such a system can enhance capacity in areas with high traffic density. This capacity can be further optimized by carefully managing the interference generated by beam allocations. The proposed algorithm illustrates a strategy of dividing the available bandwidth between two beams that share grating lobes at their positions. Additionally, after the initial beam allocation, the paper outlines a method to redistribute the beams more evenly across different frequency bands, ensuring a balanced interference load in each band. The resource allocation problem involves complex optimization of both interference and available bandwidth. Future work could enhance the algorithm by incorporating detailed interference analysis to account for complex interactions between beams and grating lobes. This includes evaluating interference from grating lobes at varying energy levels and exploring aperture tapering techniques to mitigate their effects. Additionally, future studies should analyze real-world scenarios with non-uniform user distributions to better understand system performance under practical conditions.

Acknowledgment

This project has received funding from the European Union's Horizon 2020 research and innovation program under the Marie Skłodowska-Curie grant agreement No 101072798.

References

[1] 3GPP TR 38.811, "NR for Future Wireless Networks"
[2] P. Angeletti, R. De Gaudenzi, "Heuristic Radio Resource Management for Massive MIMO in Satellite Broadband Communication Networks" IEEE Access, October 2021.
[3] G.Orlando, M.Pellet, G.Goussetis, T.Deleamotte, H.Legay, "Optimizing communication capabilities in Non-Terrestrial Network: A comparative analysis of continuous and Distributed Aperture Solutions." November 2024.
[4] D. Tuzi, T. Delamotte, A. Knopp. "Beamforming Schemes for 6G Direct-to-Cell Connectivity Using Satellite Swarms," in 18th European Conference on Antennas and Propagation (EuCAP), March 2024.
[5] P. Angeletti, R. De Gaudenzi, "Optimizing Massive MIMO Design for Non Uniform Traffic in Broadband Telecommunication Satellites Networks" IEEE Access, October 2023.
[6] P. Angeletti, R. De Gaudenzi, "Virtual Distancing: A Beam-Steering Technique for Interference Reduction in Multibeam Antennas", IEEE International Symposium on Phased Array Systems and Technology, 2022
[7] M. Pellet, G. Goussetis, J. Mota, H. Legay and F. Vidal. "Multibeam coverage optimization for broadband satellites with hybrid beamforming direct radiating arrays," in *IEEE International Symposium on Antennas and Propagation*, July 2023.
[8] M. Pellet, G. Goussetis, J. Mota, H. Legay and F. Vidal. "Multibeam Phased Arrays Exploiting Frequency Dispersion for Massive MIMO Satellite Communications" in *18th European Conference on Antennas and Propagation (EuCAP)*, April 2024.
[9] F. Vidal, H. Legay, G. Goussetis and JP. Fraysse. "Joint Precoding and Resource Allocation Strategies Applied to a Large Direct Radiating Array for GEO Telecom Satellite Applications," in *15th European Conference on Antennas and Propagation (EuCAP)*, March 2021.
[10] 3GPP. "Release 17." 3gpp.org. Accessed: Oct. 5, 2023. [Online]. Available: https://www.3gpp.org/specifications-technologies/releases/release-17
[11] R. J. Mailloux, "Phased Array Antenna Handbook", 2nd ed. Norwood, MA, USA: Artech House, 2005.
[12] C. A. Balanis. "Antenna Theory Analysis And Design," *Phil. Trans. Roy. Soc. London*, 4th ed., 2016.